RSC Advances

ROYAL SOCIETY OF CHEMISTRY

www.rsc.org/advances

Journal Name

ARTICLE

Rational design of hierarchical Ni embedded NiO hybrid nanospheres for high-performance lithium-ion batteries

Received 00th January 20xx,
Accepted 00th January 20xx

DOI: 10.1039/x0xx00000x

www.rsc.org/

Na Feng[a], Xiaolei Sun[b], Hongwei Yue[c] and Deyan He[c,*]

Novel hierarchical Ni/NiO hybrid nanospheres were fabricated by a simple solvothermal synthesis followed by a thermal oxidation. The hybrid nanospheres are uniform-sized and composed of tiny Ni embedded NiO nanoparticles. Galvanostatic battery tests show that the corresponding electrode can deliver a high reversible capacity of 712 mA h g^{-1} for the second discharge and a capacity of 825 mA h g^{-1} was obtained after 132 cycles at a rate of 0.2 C. Good rate performance was achieved even when the rate is as high as 12 C with a high capacity of 453 mA h g^{-1}, and a capacity of 800 mA h g^{-1} was retained when it returned to 0.2 C after 300 cycles. The excellent cycling stability and rate performance are derived from the special nanostructural characteristics of the prepared hybrid nanospheres, indicating that they are a promising anode material for high-performance lithium-ion batteries.

Introduction

Electrochemical energy storage is currently the most versatile technology because of its flexibility to cover wide energy and time domains. Lithium-ion batteries (LIBs) are the dominant power source for implantable medical devices, hybrid electric vehicles and electric vehicles.[1-4] However, the energy density of the commercial LIBs is not sufficient for long range electric vehicles. To meet the extensive demands, diverse electrode materials should be developed with high reversible capacity, excellent rate capability, and superior cycling stability.[5]

Transition metal oxides, such as CuO,[6, 7] Co_3O_4,[4, 8] Fe_2O_3,[9,10] and NiO[11] are the more promising candidates which exhibit large reversible capacities. However, despite their high capacities, the practical application of these anode materials always suffers from the rapid capacity fading because of their poor conductivity and large volume changes over the cycling process. One promising approach to break through these limitations is to hybridize carbonaceous or metallic materials for improving the conductivity[12-14] and fabricate nanostructured materials for accommodating the strain during volume changes[15-18]. Especially, three-dimensional (3D) nanostructures have been proved to be effective in improving electrochemical properties. The improvement profits from their easy accessibility for the electrolyte with large surface-to-volume ratio which can offer more connecting opportunities and positions with the electrodes, accelerate phase transition and restrain the crumbling and cracking of the electrode, and the 3D nanostructures can shorten path length for lithium ion transportation, favouring the physical and chemical interactions of the electrodes and lithium ions.[19-21] Nickel oxide as a metal deficient p-type semiconductor has attracted considerable attention due to its high theoretical capacity (718 mA h g^{-1}), low cost, environmental friendliness, and natural abundance.

Herein, we report a simple solvothermal method with a subsequent thermal oxidation to synthesize hierarchical Ni embedded NiO hybrid nanospheres. It was shown that the material exhibits high capacity, excellent cycling stability and rate capability. The Ni/NiO hybrid nanospheres have been thought to enhance their capacity retention by the special 3D and hierarchical nanostructures.

Experimental

Fabrication procedure

Hierarchical Ni/NiO hybrid nanospheres were fabricated by a two-step approach of solvothermal synthesis of Ni nanospheres and subsequent thermal oxidation in air. All the analytical grade reagents were used without further purification. In a typical synthesis procedure of precursory Ni nanospheres, 1.5 mmol $NiCl_2 \cdot 6H_2O$ for providing Ni ion and 3 mL hydrazine hydrate ($N_2H_4 \cdot H_2O$) as strong reducing agent were dissolved in 30 mL ethylene glycol (EG) solvent with 1 mmol cetyltrimethyl ammonium bromide (CTAB) as crystal modifier. Then the clear solution was transferred into a Teflon-lined stainless steel autoclave. It was maintained at 170 °C for 4 h and then cooled naturally to room temperature. The resultant gray black Ni nanospheres were centrifuged, rinsed with deionized water and ethanol for several times, dried at 60 °C and then heated to 600 °C at a rate of 5 °C min^{-1} and held for 4 h in a horizontal tube furnace in air.

Structural characterization

[a] Northwest Institute of nuclear technology, Xi'an,710024,China
[b] Leibniz Institute for Solid State and Material Research, Dresden, Germany
[c] School of Physical Science and Technology, and Key Laboratory for Magnetism and Magnetic Materials of the Ministry of Education, Lanzhou University, Lanzhou, 730000, China. E-mail: hedy@lzu.edu.cn; Fax: +86-931-8913554; Tel: +86-931-8912546

The structures and morphologies of the fabricated Ni/NiO hybrid nanospheres were characterized by X-ray powder diffraction (XRD, Rigaku RINT2400 with Cu Kα radiation), micro-Raman spectrometer (Jobin-Yvon LabRAM HR800 UV) with a radiation of 532 nm, field-emission scanning electron microscopy (FE-SEM, Hitachi, S-4800) and transmission electron microscopy (TEM, FEI, Tecnai G2 F30) equipped with an energy-dispersive X-ray spectroscopy (EDX), respectively. Thermogravimetric analysis (TGA) was carried out in air at a heating rate of 5 °C min^{-1} using a Perkin Elmer Diamond TGA instrument.

Electrochemical characterization

Electrochemical characterizations were carried out using CR-2032-type coin cells assembled in a high-purity argon-filled glovebox (H_2O, O_2 < 0.5 ppm, MBraun, Unilab) with lithium foil as the counter and reference electrode. Celgard 2320 was used as separator membrane. The working electrode was consisted of the electrode material, acetylene black (AB), and sodium alginate (SA) binder at a weight ratio of 8: 1: 1. The electrolyte was 1 M lithium hexafluorophosphate ($LiPF_6$) dissolved in ethylene carbonate : dimethyl carbonate : ethyl methyl carbonate in a 1:1:1 volume ratio. The galvanostatic discharge-charge cycling test, cyclic voltammetry (CV) and electrochemical impedance spectroscopy (EIS) measurements were carried out at room temperature by using a multichannel battery tester (Neware BTS-610) and an electrochemical workstation (CHI 660C), respectively.

Results and discussion

Structural characterization

The crystal structure and phase composition of Ni and Ni/NiO nanospheres were confirmed by XRD measurement. Fig. 1a shows typical XRD patterns of Ni nanospheres before and after thermal oxidation with the standard diffraction patterns. The synthesized Ni nanospheres exhibits the peaks of (111), (200), and (220), which are the characteristic peaks of metallic Ni (JCPDS 04-0850, space group $Fm\bar{3}m$ (225), a = 3.524 Å).[8] The XRD peaks after the thermal oxidation consist of NiO and Ni phases, indicating the formation of the Ni/NiO hybrid. The new diffraction peaks can be well indexed to the data of cubic NiO (JCPDS 44-1159, space group $Fm\bar{3}m$ (225), a = 4.178 Å).[22] Fig. 1b shows the micro-Raman spectra of Ni and Ni/NiO nanospheres. No signal can be found for the Ni nanospheres, showing that the synthesized precursor had not been oxidized. The Raman spectrum of the Ni/NiO nanospheres exhibits several bands in the region above 100 cm^{-1}, including TO and LO modes (~159 cm^{-1}) due to one-phonon (1P), 2TO modes (~363 cm^{-1}), TO + LO (~533 cm^{-1}), and 2LO (~698 cm^{-1}) modes due to two-phonon (2P). The strongest band at 1066 cm^{-1} is due to a two-magnon (2M) scattering. The bands for NiO are well observed at room temperature, 1P band is due to the presence of defects or surface effect, 2M scattering involves Brillouin zone-edge magnons, interacting weakly with phonons.[23]

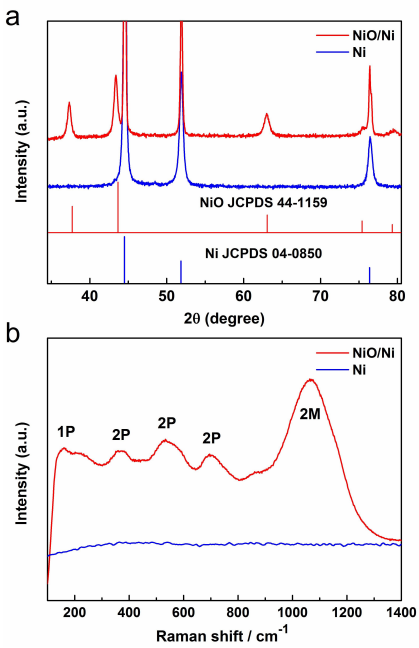

Fig. 1 (a) XRD spectra of Ni and hierarchical Ni/NiO nanospheres with standard diffraction patterns. (b) micro-Raman spectra of Ni and Ni/NiO nanospheres.

The morphologies of the Ni and Ni/NiO nanospheres were observed by SEM. It shows that the samples have a perfect 3D netlike structure made up of nanosphere-based short chains. The local magnification shows that the samples display a chainlike structure which is composed of the closely interconnected nanospheres. The nanospheres are uniform with a narrow size distribution. The average diameters of the precursory Ni nanospheres and Ni/NiO hybrid nanospheres are estimated to be ~400 nm and ~500 nm, respectively. The average diameter of the Ni/NiO nanospheres becomes larger because of the mass increase and the density decrease of NiO after oxidation. Also, the surface of the nanospheres becomes much coarser as a result of the solid phase crystallization during oxidation.

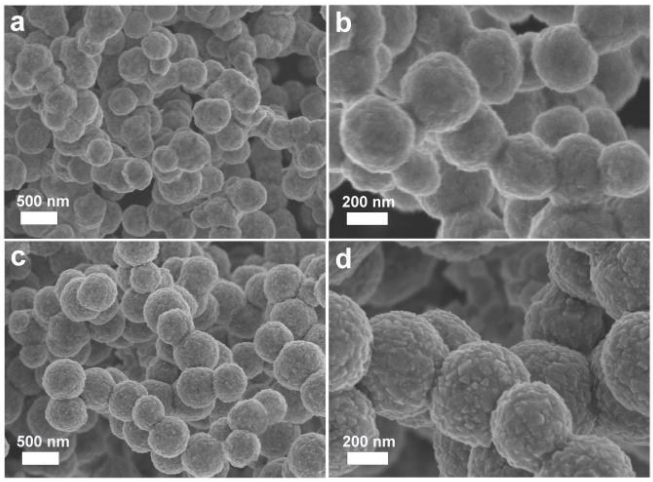

Fig. 2 Low- and high-magnification SEM images of (a, b) precursory Ni nanospheres and (c, d) hierarchical Ni/NiO nanospheres.

To accurately reveal the microstructure of the prepared Ni/NiO nanospheres, TEM characterizations were carried out. Fig. 3a shows representative TEM image of the Ni/NiO nanospheres. The product is composed of uniform nanospheres with diameter of ~400 nm. The high-magnification TEM image in the inset shows that the inner of the nanosphere is prominently wrinkly. The high-resolution (HR-) TEM image shown in Fig. 3b was taken focusing on the rectangle area in the inset of Fig. 3a. The lattice fringe can be clearly seen and the spacings were determined to be 0.241 and 0.203 nm, corresponding to the planes of cubic $(101)_{NiO}$ and $(111)_{Ni}$, respectively. Furtherly, we can draw a conclusion that the hierarchical nanospheres are consisted of multi-nanoparticles, each nanoparticle is consisted of Ni embedded NiO nanostructures. The selected-area electron diffraction (SAED) pattern (Fig. 3c) taken from the circled area in Fig. 3a shows the distinct spotty rings, revealing a highly polycrystalline cubic nanostructures. According to the diffraction pattern, the measured lattice constants and interplanar spacings are well matched with Bragg reflection of (110), (012), and (101) planes corresponding to cubic NiO and (220) planes to Ni phase, which agree well with the obtained XRD results. Semi-quantitative EDX analysis (Fig. 3d) was applied to determine the chemical composition of the sample. Nickel and oxygen elements were detected with a quantitative molar ratio of ~ 2:1 (Ni:O), confirming that the as-prepared product contains NiO and Ni. The signals of C and Cu come from the sample holder.

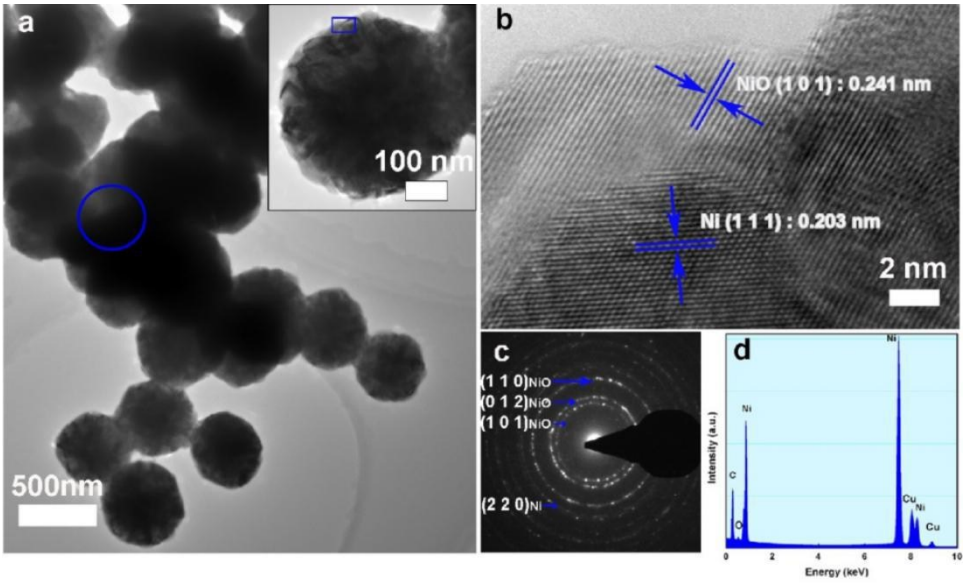

Fig. 3 (a) TEM image of the hierarchical Ni/NiO nanospheres, the inset is a high-magnification TEM image for a single nanosphere. (b) HR-TEM image taken from the rectangle marked area in the inset of (a). (c) The SAED pattern from the area indicated by the circle shown in (a). (d) The corresponding EDX spectrum.

Following steps can be proposed in understanding the formation of Ni nanospheres. Numerous tiny Ni crystalline nuclei were generated at the initial step. Due to their high surface energies, the adjacent nuclei preferred to coalesce and grow into primary nanoparticles. The nanoparticles further aggregated into spheres, and continued to grow by combining with the remaining primary particles in the presence of CTAB. Finally, hierarchical nanospheres assembled by Ni nanoparticles formed as a result of the magnetic dipole-dipole interaction and the CTAB effect. Each Ni nanoparticle has been oxidized into Ni/NiO nanostructure after the thermal oxidation. The schematic mechanism for the formation of the hierarchical Ni/NiO hybrid nanospheres is shown in Scheme 1. The oxidation mechanism of Ni was also investigated. As the oxidation temperature decreases (< 1000 °C), the kinetics gradually change into a sub-parabolic behavior, which means that the oxidation rate decreases faster as a function of time than as for high-temperature parabolic kinetics, record as $\propto t^{1/>2}$.[24] The active mass of NiO was weighed by a microbalance (Mettler, XS105DU) with an accuracy of 0.01 mg. According to the reaction of $2Ni + O_2 = 2NiO$, the active weight of NiO (m_{NiO}) is derived from $m_{NiO} = \Delta m \times 74.69/16$, where Δm is the weight difference of Ni nanospheres before and after oxidation. The weight ratio of NiO : Ni is calculated to be 73.3 : 26.7 in the hybrid.

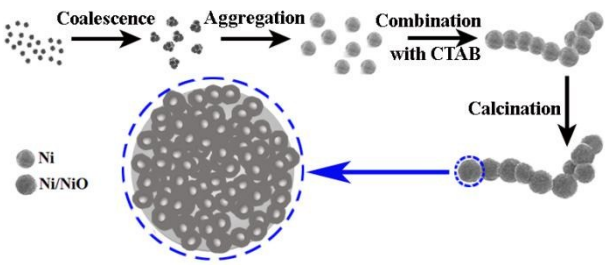

Scheme 1 Schematic mechanism for the formation of the hierarchical Ni/NiO hybrid nanospheres.

Thermogravimetric analysis (TGA) was performed to determine the mass contents of NiO and Ni in the hybrid. The recorded TGA curve is shown in Fig. 4, which was carried out

in air from 40 to 1000 °C with a heating rate of 5 °C min^{-1}. We estimate that the low heating rate with enough time and the high temperature can ensure Ni be oxidized completely. The weight increase over the temperature range of 380~720 °C is attributed to the oxidation of nickel in the hybrid. From the overall weight increment (6.65 %) of the final product, the weight ratio of NiO : Ni is calculated to be 75.6 : 24.4 in the hybrid. This result is in agreement with 73.3% of NiO determined by weight difference before and after the oxidation.

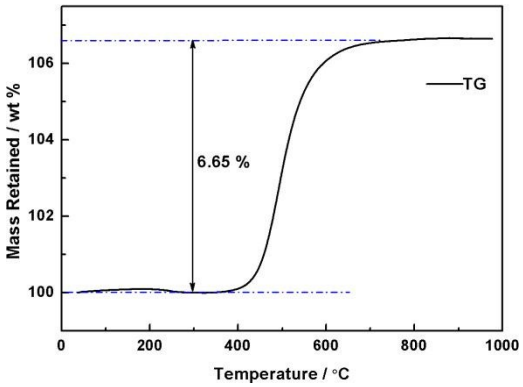

Fig. 4 TGA curve of the hierarchical Ni/NiO nanospheres.

Electrochemical performance

Representative electrochemical behavior of the hierarchical Ni/NiO nanospheres electrodes was investigated by cyclic voltammetry in the voltage range of 0.01-3.0 V *vs.* Li^+/Li at a scan rate of 0.1 mV s^{-1}. In the first cathodic scan in Fig. 5a, the broad cathodic peak at ~0.41 V corresponds to the initial reduction of NiO to Ni ($NiO + 2Li^+ + 2e^- \rightarrow Ni + Li_2O$), and preliminary decomposition of the electrolyte to form a partially reversible solid electrolyte interphase (SEI).[25, 26] During the first anodic scan, two oxidation peaks are found at 1.56 and 2.19 V. The weak peak at 1.56 V corresponds to the decomposition of the organic SEI component, the peak around 2.19 V is related to the NiO formation and Li_2O decomposition ($Ni + Li_2O \rightarrow NiO + 2Li^+ + 2e^-$).[12, 27] The cathodic peak shifts to about 1.21 and the anodic peak to 2.22 V for the subsequent cycles due to the drastic lithium driven, structural or textural modifications during the first lithiation.[19] The CV curves are quite similar after the first cycle, suggesting that the stable electrochemical process has been set up.

Fig. 5b shows the initial three charge-discharge voltage profiles at a rate of 0.2 C (1 C is defined as 718 mA g^{-1} for NiO.[27]). A long wide plateau around 0.72 V followed by a sloping curve was observed in the first discharge curve, which is attributed to the reduction of NiO to Ni.[28] The discharge plateau shifts to around 1.30 V in the subsequent discharge processes, while the charge plateau shifts from 2.16 V to 2.22 V, which are well in agreement with the CV results shown in Fig. 5a. The initial discharge and charge capacities were found to be 1040 and 720 mA h g^{-1}, respectively. The irreversible capacity loss can be mainly attributed to the interfacial reactions between the electrode and electrolyte, which could be improved by prelithiation in future studies.[29]

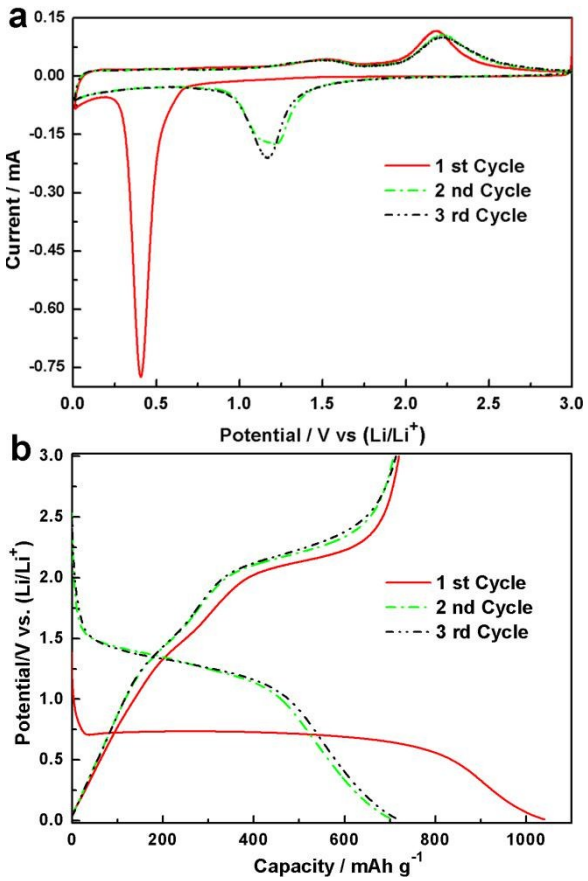

Fig. 5 Electrochemical performance of the hierarchical Ni/NiO nanospheres electrodes. (a) CV curves at a scan rate of 0.1 mV s^{-1}. (b) Galvanostatic charge–discharge voltage profiles for the initial three cycles at 0.2 C.

The capacity retention and the corresponding coulombic efficiency of the galvanostatic test run at 0.2 C are shown in Fig. 6a. It can be seen that the capacity of the electrode has excellent retention, it shows a slight increase and reaches 825 mA h g^{-1} after 125 cycles. The increasing specific capacity can be ascribed to the reversible growth of a polymeric SEI film resulting from kinetically activated electrolyte degradation.[19] It is observed that the coulombic efficiency is more than 98% since the second cycle.

To further investigate the high power performance of the hierarchical Ni/NiO nanospheres electrodes, the rate capability has been evaluated. Fig. 6b shows the charge-discharge voltage profiles at various C rates. It can be seen that, with the rate increases, the discharge potential decreases and the charge potential increases due to kinetic effects of the active material. Fig. 6c shows the capacity retention at various C rates after 132 cycles at 0.2 C. After 132 cycles, the discharge capacity reaches about 825 mA h g^{-1}, it slightly reduces to 735, 654, 553 and 453 mA h g^{-1} at rates of 1 C, 2 C, 6 C, and 12 C, respectively. Even at the high rate of 12 C, the capacity is still much higher than the theoretical limit of graphite. More importantly, when the current rate is set back to 0.2 C, the capacity can recover to the initial value of ~800 mA h g^{-1} after 300 cycles, again indicating that the hierarchical Ni/NiO nanospheres electrode is of excellent capacity retention at high rates. These results suggest that the electrodes of the hierarchical Ni/NiO nanospheres are

quite stable and reversible for cycling. Table 1 shows a comparison of the electrochemical performances between the present work and those reported in the literatures[12, 13, 27, 30-32]. It is worth noting that the hierarchical Ni/NiO nanospheres electrodes show a significant improvement with better capacity retention and rate capability.

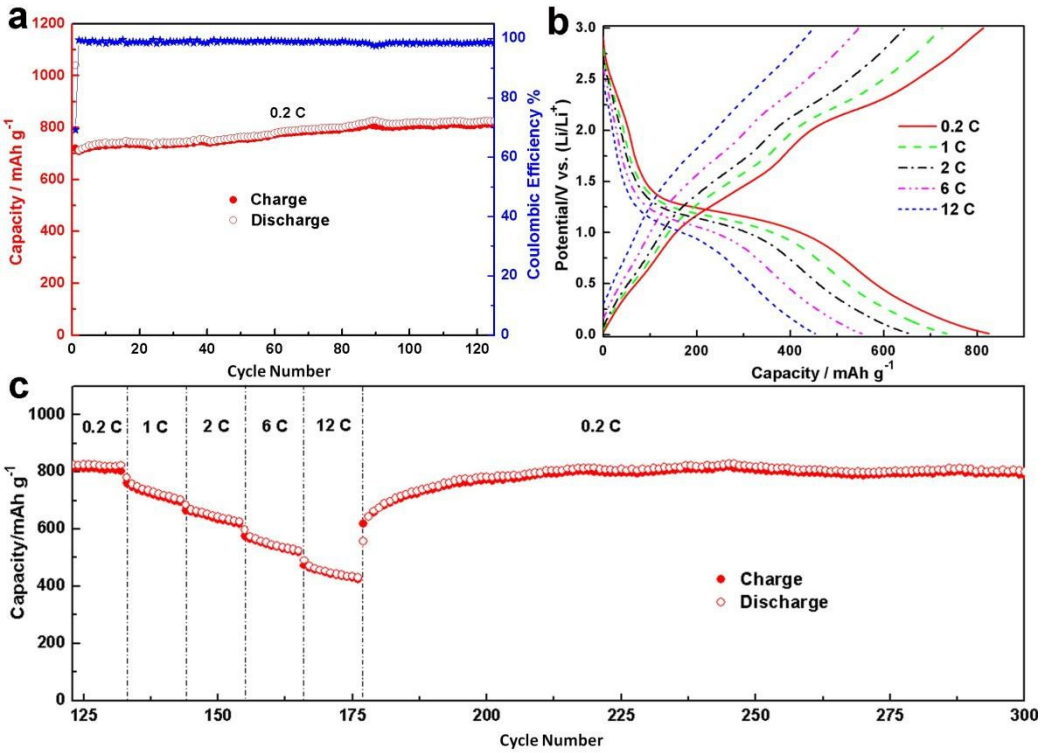

Fig. 6 Electrochemical performance of the hierarchical Ni/NiO nanospheres electrodes. (a) Capacity retention and coulombic efficiency of the galvanostatic test run at 0.2 C. (b) The representative charge–discharge voltage profiles at various C rates. (c) Rate capability of the Ni/NiO nanospheres electrode at various C rates from 0.2 C to 12 C.

Table 1 Comparison of the electrochemical performances of the hierarchical Ni/NiO nanospheres in this work with those reported in the literatures.

Electrode material	Current density	1st charge/discharge capacity (mA h g-1)	Coulombic efficiency	Cyclability (mA h g-1)/ cycle times	Applied potential range (V)	Rate capacity (mA h g-1)/ current density	Ref.
NiO hollow microspheres	200 mA g-1	1569.4 /975.1	37.8%	380 /30	0.02~3.0	200 /600 mA g-1	12
NiO graphene nanosheets	200 mA g-1	2169.6 /1476.2	67.6%	704.8 /50	0.01~3.0	403.3 /1600 mA g-1	13
NiO graphene hybrid	100 mA g-1	~1125 /~750	66.7%	646.1 /35	0.02~3.0	368.5 /800 mA g-1	30
Co-doped NiO nanoflake arrays	100 mA g-1	1201 /882	73.4%	589.5 /50	0.01~3.0	471 /2000 mA g-1	31
Curved NiO nanomembranes	0.2 C	1073 /732	68.2%	710 /110	0.02~3.0	374 /10 C 240 /20 C	27
NiO-Ni nanocomposite	100 mA g-1	1152.4 /820.5	71.2%	<650 /50	0.02~3.0	/	32
Hierarchical Ni/NiO hybrid nanospheres	0.2 C	1040.0 /719.9	69.2%	825.3 /132	0.01~3.0	453.1 /12 C	**Present work**

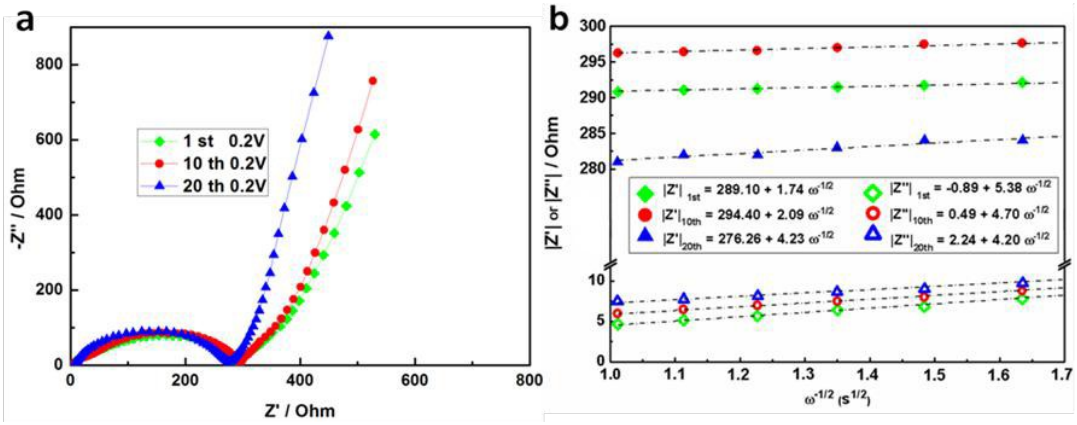

Fig. 7 (a) Nyquist plots of the hierarchical Ni/NiO nanospheres electrode after different discharge cycles at 0.2 V *vs.*Li^+/Li. (b) Plotting of real (solid symbols) and imaginary (hollow symbols) resistance *vs.* inverse square root of the angular frequency $\omega^{-1/2}$ at 0.2 V *vs.* Li^+/Li after the 1st, 10th and 20th cycle, respectively. The dot lines are the linear fitting for the obtained data.

In order to better understand the superior electrochemical performance of the hierarchical Ni/NiO nanospheres electrodes, electrochemical impedance spectra of the cells after different cycles were measured at 0.2 V *vs*. Li^+/Li. Fig. 7a shows Nyquist plots of the electrode after the 1st, 10th and 20th cycle. As it is well-known, the charge transfer resistance R_{ct} represents the total resistance at the interface between the electrode and the electrolyte, indicating fast lithium intercalation kinetics. The solution resistance R_s and charge-transfer resistance R_{ct} can be obtained from the Nyquist plots, where the high frequency semicircle intercepts the real axis at R_s and (R_s + R_{ct}), respectively. Compared the corresponding results, the solution resistance R_s was measured to be 5.7, 6.6, and 5.6 Ω, respectively, while the charge transfer resistances R_{ct} are respectively 290.8, 289.6 and 270.5 Ω at 0.2 V for the 1st, 10th and 20th cycle with little variation, which can be ascribed to the stable interface between the special hierarchical nanostructures and the electrolyte. Warburg impedance is related to the diffusion of lithium ions, the lithium diffusion part is located in the linear zone of the corresponding to the low frequency region. Fig. 7b shows the real and imaginary Warburg resistances after the 1st, 10th and 20th cycle. The conventional Warburg impedance Z_W is expressed as $Z_W = (\sigma_r - j\sigma_i)\ \omega^{-1/2}$, in which σ_r is the real part of Warburg coefficient and σ_i the imaginary part. It can be seen that all the real and imaginary part of Warburg coefficients of these different cycles are lower and have similar dependence on the measured frequency (as denoted by the formulae in Fig. 7b), showing a good cycling stability. Also, it indicates that the material structure inside the cell shows no change through 20 cycles.

The SEM images of the electrode after various C rates cycles are shown in Fig. 8. It can be seen that the morphology of the nanospheres is almost maintained and no obvious crush or collapse can be found even after 300 cycles at high rates. The size of the nanospheres becomes larger and is estimated to be ~800 nm, which may be attributed to the formation of SEI film after discharge cycling test and volume expansion of NiO.

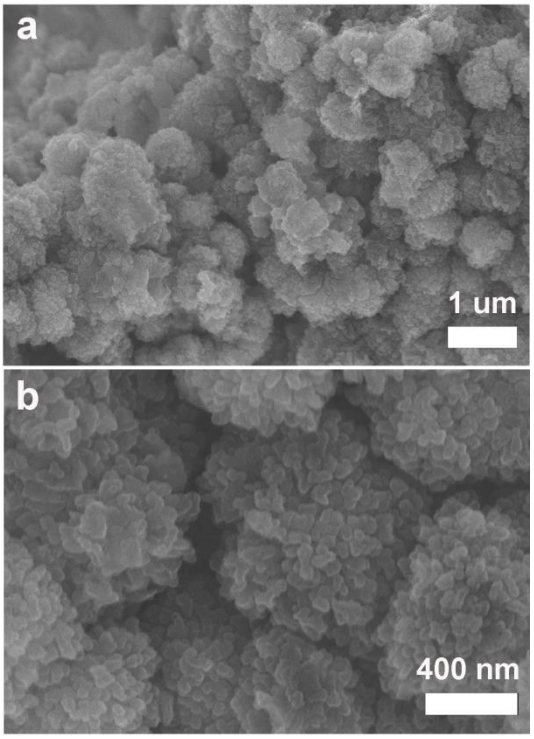

Fig. 8 (a) Low- and (b) high-magnification SEM images of the hierarchical Ni/NiO nanospheres electrode after 300 cycles at various C rates.

The high capacity and excellent rate capability and cycling stability of the hierarchical Ni/NiO nanospheres electrodes can be attributed to the special material structure of the hierarchical nanospheres consisted of Ni embedded NiO nanoparticles. Such a 3D nanostructure with large surface-to-volume ratio can provide space for volume expansion and preserve the integrity of the structure during lithiation. Furthermore, the inner Ni embedded NiO nanoparticle architecture can limit the motion and agglomeration of the particles during cycling, which may endure the volume expansion/contraction during redox reactions. Therefore, when used as an anode in LIBs, the hierarchical Ni/NiO nanospheres demonstrated much higher rate capacities and better cycling performance than other

Ni/NiO materials.[33-35] This unique architecture provides a tremendous opportunity to improve electrochemical properties. Further work should be done to decrease the Ni content to achieve the optimum performance.

Conclusions

In summary, the hierarchical Ni/NiO nanospheres have been fabricated by a facile solvothermal growth and a subsequent calcination. As an electrode material for LIBs, it exhibits high capacity, excellent rate capability and cyclic stability. A high reversible capacity of 825 mA h g^{-1} after 132 cycles at a rate of 0.2 C and a reversible capacity of 453 mA h g^{-1} at a rate as high as 12 C made the material a promising candidate for anode materials of high-power LIBs, and it is envisaged that such a 3D hierarchical morphology could find its interesting applications in other fields.

Acknowledgements

This work was supported by the National Natural Science Foundation of China with grant No. 11179038.

Notes and references

1. K. T. Nam, D. W. Kim, P. J. Yoo, C. Y. Chiang, N. Meethong, P. T. Hammond, Y. M. Chiang and A. M. Belcher, *Science*, 2006, **312**, 885-888.
2. Y. H. Zhang, L. Guo, L. He, K. Liu, C. Chen, Q. Zhang and Z. Wu, *Nanotechnology*, 2007, **18**, 485609.
3. E. Hosono, T. Kudo, I. Honma, H. Matsuda and H. Zhou, *Nano Lett.*, 2009, **9**, 1045-1051.
4. X. W. Lou, D. Deng, J. Y. Lee, J. Feng and L. A. Archer, *Adv. Mater.*, 2008, **20**, 258-262.
5. J. B. Dunn, L. Gaines, J. C. Kelly, C. James and K. G. Gallagher, *Energy Environ. Sci.*, 2015,**8**, 158-168.
6. Q. B. Zhang, J. X. Wang, D.G. Xu, Z. X. Wang, X. H. Li and K. L. Zhang, *J. Mater. Chem. A*, 2014,**2**, 3865-3874.
7. Y. Z. Fan, R. M. Liu, W. Du, Q. Y. Lu, H. Pang and F. Gao, *J. Mater. Chem.*, 2012,**22**, 12609-12617.
8. L. L. Jin, X. W. Li, H. Ming, H. H. Wang, Z. Y. Jia, Y. Fu, J. Adkins, Q. Zhou and J. W. Zheng, *RSC Adv.*, 2014,**4**, 6083-6089.
9. S. Chen, Y. L. Xin, Y. Y. Zhou, F. Zhang, Y. R. Ma, H. H. Zhou and L. M. Qi, *J. Mater. Chem. A*, 2015,**3**, 13377-13383.
10. Y. Zhao, J. Li, Y. Ding and L. Guan, *Chem. Commun.*, 2011, **47**, 7416-7418.
11. X. L. Sun, Ch. L. Yan, W. P. Si, J. W. Deng and O. G. Schmidt, *Adv. Energy Mater.*, 2014, **4**, 1300912.
12. D. Xie, W. W. Yuan, Z. M. Dong, Q. M. Su, J. Zhang and G. H. Du, *Electrochim. Acta*, 2013,**92**, 87-92.
13. D. Xie, Q. M. Su, W. W. Yuan, Z. M. Dong, J. Zhang and G. H. Du, *J. Phys. Chem. C.,* 2013, **117**, 24121−24128.
14. Q. Q. Xiong, J. P. Tu, X. H. Xia, X. Y. Zhao, Ch. D. Gu and X. L. Wang, *Nanoscale*, 2013, **5**, 7906–7912.
15. G. Zhang, Y. Chen, B. Qu, L. Hu, L. Mei, D. Lei, Q. Li, L. Chen, Q. Li and T. Wang, *Electrochim. Acta*, 2012, **80**, 140-147.
16. P. Roy and S. K. Srivastava, *J. Mater. Chem. A*, 2015,**3**, 2454-2484.
17. J. Jiang, Y. Li, J. Liu and X. Huang, *Nanoscale*, 2011, **3**, 45-58.
18. T. Yang and B. A. Lu, *Phys. Chem. Chem. Phys.*, 2014, **16**, 4115-4121.
19. X. Li, D. Li, L. Qiao, X. Wang, X. Sun, P. Wang and D. He, *J. Mater. Chem.*, 2012, **22**, 9189-9194.
20. K.Huang and Q.Zhang, *Nano Energy*, 2012, **1**, 172-175.
21. Q. Xia, H. L. Zhao, Z. H. Du, Z. J. Zhang, S. M. Li, C. H. Gao and K. Świerczek, *J. Mater. Chem. A*, 2016,**4**, 605-611.
22. X. Li, A. Dhanabalan and C. Wang, *J. Power Sources*, 2011, **196**, 9625-9630.
23. N. Mironova-Ulmane, A. Kuzmin, I. Steins, J. Grabis, I. Sildos and M. Pärs, *Journal of Physics: Conference Series*, 2007, **93**, 012039.
24. R. Haugsrud, *Corros. Sci.*, 2003, **45**, 211-235.
25. X. H. Huang, J. P. Tu, C. Q. Zhang and F. Zhou, *Electrochim. Acta*, 2010, **55**, 8981-8985.
26. D. Xie, Q. M. Su, Z. M. Dong, J. Zhang and G. H. Du, *CrystEngComm*, 2013,**15**, 8314-8319.
27. X. L. Sun, W. P. Si, X. H. Liu,J. W. Deng, L. X. Xi and O. G. Schmidt, *Nano Energy*, 2014,**9**,168-175.
28. X. Wang, Z. Yang, X. Sun, X. Li, D. Wang, P. Wang and D. He, *J. Mater. Chem.*, 2011, **21**, 9988-9990.
29. N. Feng, S. Peng, X. Sun, L. Qiao, X. Li, P. Wang, D. Hu and D. He, *Mater. Lett.*, 2012, **76**, 66-68.
30. Y. J. Mai, S. J. Shi, D. Zhang, Y. Lu, C. D. Gu and J. P. Tu, *J. Power Sources*, 2012, **204**, 155-161.
31. Y. J. Mai, J. P. Tu, X. H. Xia, C. D. Gu and X. L. Wang, *J. Power Sources*, 2011, **196**, 6388-6393.
32. X. H. Hang, J. P. Tu, B. Zhang, C. Q. Zhang, Y. Li, Y. F. Yuan and H. M. Wu, *J. Power Sources*, 2006, **161**,541-544.
33. H. Liu, G. Wang, J. Liu, S. Qiao and H. Ahn, *J. Mater. Chem.*, 2011, **21**, 3046-3052.
34. B. Wang, J. L. Cheng, Y. P. Wu, D. Wang and D. N. He, *Electrochem. Commun.*, 2012, **23**, 5-8.
35. F. Cao, F. Zhang, R. Deng, W. Hu, D. Liu, S. Song and H. Zhang, *CrystEngComm*, 2011, **13**, 4903-4908.

Rational design of hierarchical Ni embedded NiO hybrid nanospheres for high-performance lithium-ion batteries

Na Feng[a], Xiaolei Sun[b], Hongwei Yue[c] and Deyan He[c,*]

The uniform-sized Ni embedded NiO nanospheres exhibit high capacity of 453 mAh g^{-1} (12C) and 800 mA h g^{-1} (0.2C) after 300 cycles.

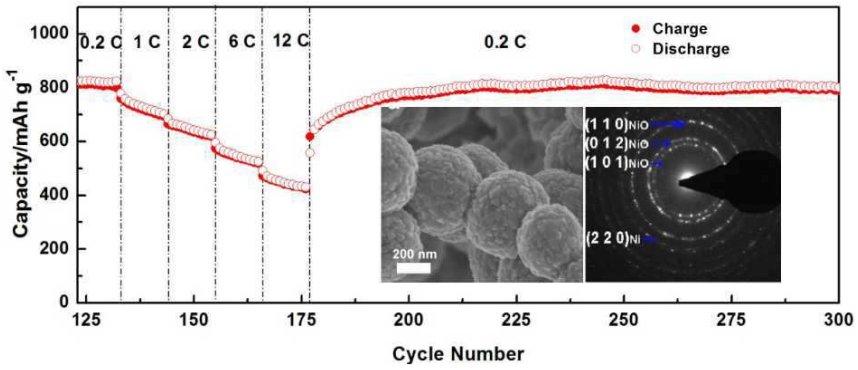

[a] Northwest Institute of nuclear technology, Xi'an,710024,China

[b] Leibniz Institute for Solid State and Material Research, Dresden, Germany

[c] School of Physical Science and Technology, and Key Laboratory for Magnetism and Magnetic Materials of the Ministry of Education, Lanzhou University, Lanzhou, 730000, China. E-mail: hedy@lzu.edu.cn; Fax: +86-931-8913554; Tel: +86-931-8912546